Fully Coupled Aero-Hydrodynamic Simulation of Floating Offshore Wind Turbines with Overset Grid Technology

Ping Cheng and Decheng Wan

Abstract The fully coupled aero-hydrodynamic simulation of the OC4 Phase II semi-submersible floating offshore wind turbine (FOWT) is conducted. The three-dimensional (3D) Reynolds-Averaged Navier–Stokes (RANS) equations, enclosed with the k–ω SST turbulence model are solved. The in-house code naoe-FOAM-SJTU solver, based on OpenFOAM and coupled with overset grid technology, is employed. The aerodynamic forces which decrease with the coupling effect of platform motions oscillate in wave period. With the aerodynamic forces applying on the platform through tower, the platform motions show significant variation on the equilibrium position of surge and pitch DOFs. Detailed flow information also clarities the flow fields and indicates the coupling effects.

Keywords Fully coupled Aero-hydrodynamic simulation
Floating offshore wind turbine (FOWT) · Overset grid technique
Naoe-FOAM-SJTU solver

1 Introduction

Floating offshore wind turbines (FOWTs) are considered more economically viable compared to bottom-fixed ones when water depth is larger than approximately 50 m [1]. FOWTs have attracted more attention in recent years, especially in coastal countries with enormous ocean wind energy resource. Since the first multi-megawatt FOWT in the world installed at the west coast of Norway in June 2009 [2], more FOWTs have been designed and served for coastal cities [3]. However, designing FOWT system is still a quite challenging task due to the complicated structure, the complex environmental loading, and the coupling effects.

P. Cheng · D. Wan (✉)
State Key Laboratory of Ocean Engineering, School of Naval Architecture, Ocean and Civil Engineering, Collaborative Innovation Center for Advanced Ship and Deep-Sea Exploration, Shanghai Jiao Tong University, 200240 Shanghai, China
e-mail: dcwan@sjtu.edu.cn

© Springer Nature Singapore Pte Ltd. 2019

K. Murali et al. (eds.), *Proceedings of the Fourth International Conference in Ocean Engineering (ICOE2018)*, Lecture Notes in Civil Engineering 22,
https://doi.org/10.1007/978-981-13-3119-0_42

dcwan@sjtu.edu.cn

Basic research methods consist of model test and numerical simulations. As an indispensable tool for research, model test plays an important role in study on FOWT. Model tests including intermediate-scale models monitored in offshore water areas [4] and scaled-down models tested in wave basin and wind tunnel [5] can provide more intuitionistic and practical data for further study. However, there underlies a problem that the Froude scaling law and the Reynolds similarity law cannot be guaranteed at the same time, which makes the model test data less valuable in FOWT designing. On the other hand, model test is quite expensive, especially the intermediate-scale models.

The numerical methods successfully cut down the research cost and avoid the scale effect by conducting simulations with full-scale models. Recently, fully coupled aero-hydrodynamic simulation solvers for FOWTs have been developed, which are mainly based on the traditional aerodynamic tools for fixed wind turbine and conventional hydrodynamic codes well developed in offshore ocean engineering. In early studies, most numerical tools for coupling simulation of FOWT are developed based on BEM method, such as HAWC2, 3Dfloat, etc. [6]. As is known, BEM is an empirical method with various correction models (such as Glauert correction, skewed wake correction, etc.), some researchers [7] suggested that the BEM is still questionable in unsteady aerodynamic prediction for FOWTS. Based on blade element momentum (BEM) method and potential-flow theory, the National Renewable Energy Laboratory (NREL) developed a fully coupled aero-hydro-servo-elastic tool named FAST [8]. However, depending on data-inputting from external potential-flow-based hydrodynamic solvers, such as WAMIT, restricts its usage for more accurate predictions with the viscous effect.

With rapidly developed compute technology and computing methods, more and more fully coupled studies have been conducted with CFD method. Based on OpenFOAM package, Liu [9] established a fully coupled CFD analysis tool for FOWTs and studied the coupling effect of the OC4-DeepCWind semi-submersible FOWT. Tran has also conducted the fully coupled aero-hydrodynamic analysis of this semi-submersible FOWT, while in his study a dynamic fluid body interaction approach is used [10] with Star CCM+ software combined with overset grid technique. Based on OpenFOAM, the open source CFD platform, our research team developed the CFD solver naoe-FOAM-SJTU to investigate hydrodynamic problems in the field of ship and ocean engineering. By introducing the unsteady actuator line model (UALM) [11] into OpenFOAM for aerodynamic simulation and combining with naoe-FOAM-SJTU solver, the fully coupled aero-hydrodynamic simulation model for FOWTs is established, which is named the FOWT-UALM-SJTU solver. The FOWT-UALM-SJTU solver achieves higher computational efficiency. On the other hand, the absence of accurate expression of the blades surface with refined mesh leads to lack of detailed flow information near blades, which plays critical role in deeply mechanism research. To improve the numerical accuracy, the full structured blades are directly simulated by employing overset grid technique to deal with the independent blades rotating motion and platform's 6DOFs motions problem, which is utilized in this present work.

dcwan@sjtu.edu.cn

2 Numerical Method

2.1 Governing Equations

In the numerical simulations in this paper, the incompressible Reynolds-Averaged Navier–Stokes (RANS) equations are solved, which contain the continuity equations and the momentum equations:

$$\frac{\partial U_i}{\partial x_i} = 0 \tag{1}$$

$$\frac{\partial U_i}{\partial t} + \frac{\partial}{\partial x_j}(U_i U_j) = -\frac{1}{\rho}\frac{\partial P}{\partial x_i} + \frac{\partial}{\partial x_j}\left(\nu \frac{\partial U_i}{\partial x_j} - \overline{u_i' u_j'}\right) \tag{2}$$

In these equations, U_I is the averaged flow velocity component, while u_i' is the fluctuation part; ρ is the density of the fluid; P is the pressure; ν is the kinematic viscosity.

But the equations are not closed as they contain more variables than there are equations. In order to meet the closure requirement and solve the above equations, the two-equation turbulence model k–ω SST [12] is employed, and the turbulent kinetic energy k and the turbulent dissipation rate ω can be described as:

$$\frac{\partial}{\partial \mathrm{t}}(\rho k) + \frac{\partial}{\partial x_i}(\rho k u_i) = \frac{\partial}{\partial x_j}\left(\Gamma_k \frac{\partial k}{\partial x_j}\right) + G_k - Y_k + S_k \tag{3}$$

$$\frac{\partial}{\partial \mathrm{t}}(\rho \omega) + \frac{\partial}{\partial x_i}(\rho \omega u_i) = \frac{\partial}{\partial x_j}\left(\Gamma_\omega \frac{\partial \omega}{\partial x_j}\right) + G_\omega - Y_\omega + D_\omega + S_\omega \tag{4}$$

where Γ_k and Γ_ω are the effective diffusion coefficients for the turbulent kinetic energy k and the turbulent dissipation rate ω, respectively, G_k and G_ω are turbulence generation terms for k and ω, Y_k, and Y_ω are turbulent dissipation terms for k and ω, S_k, and S_ω are the source term for k and ω, D_ω is the cross-diffusion term for ω.

2.2 Naoe-FOAM-SJTU Solver

Based on the open source CFD platform, the in-house code naoe-FOAM-SJTU solver [13, 14] is designed for computing viscous flows of ships and ocean structures. It inherits the data structure and CFD libraries in OpenFOAM, such as FVM, RANS, VOF, and PISO algorithm. The two-phase incompressible RANS equations are solved in this solver. The governing equations are discretized with finite volume method (FVM) which is capable to handle arbitrary polyhedral cells. The interface between two phases is captured using a VOF method with bounded compression technique. The turbulence models of k–ω SST and k–ε can be used for turbulence

dcwan@sjtu.edu.cn

closure. The pressure–velocity coupling equations are solved by pressure-implicit with splitting of operations (PISO) algorithm. Based on the above, a numerical tank system including wave generation and absorption module is built up, six degrees of freedom (6DOF) motion module is developed, and finally the mooring system module is added (Fig. 1).

The wave generation system is able to use boundary inlet to generate first-order regular waves and high order nonlinear waves, transient extreme waves, and freak wave. The sponge layer for wave absorption is adopted to avoid wave reflection. The mooring system module is built for hydrodynamic analysis of floating offshore structures which are moored in waters, such as semi-submersible, TLP, Spar, and FPSO. Several quasi-static models including spring, catenary, piecewise extrapolation method as well as a dynamic model lumped mass method, are utilized for simulation of mooring lines. To solve 6DOF equations, two coordinate systems are used, which are the earth-fixed coordinate system and the body-fixed coordinate system. And both dynamic deformation mesh method and overset grid technique are employed to deal with the 6DOF issues. With these modules, naoe-FOAM-SJTU solver can be applied to the simulation of ship advancing, seakeeping, superposition of complex motions, and hydrodynamics of floating platforms.

2.3 Overset Grid Technique

Using overset grid technique, the separated overlapping grids for each part with independent movement are allowed, which makes it powerful in simulating large amplitude motion problems. And the information transformation between each grid domain is built by interpolation at appropriate cells or points using DCI (domain connectivity information) which is produced by SUGGAR++ [15]. There are four main steps when using DCI in the overset grid technique: The first step is to pick out the hole cells which are located outside the simulation domain or of no interest

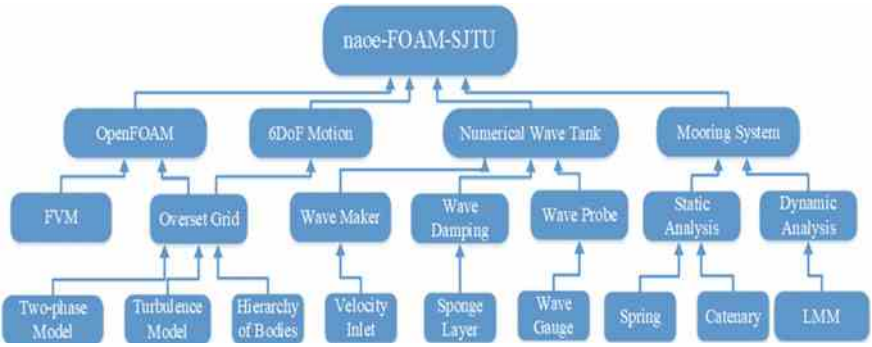

Fig. 1 Frame diagram of naoe-FOAM-SJTU solver

dcwan@sjtu.edu.cn

and exclude them from computation. As shown in Fig. 2, in overset grid, there exist series of fringe cells around hole cells, and for each fringe cell there are several donor cells which receive information from the donor cells, so the second step is to seek for the donor grids of each fringe cell and provide information from the donor grids. The third step is to obtain the value of a variable ϕ of the fringe cell by interpolation from the donor cells with:

$$\phi_I = \sum_{i=1}^{n} \omega_i \cdot \phi_i \tag{5}$$

where ϕ_I is the value of a variable ϕ of the fringe cell, ϕ_i is the value for the ith donor cell, ω_i is the dimensionless weight coefficient and follows:

$$\sum_{i=1}^{n} \omega_i = 1 \tag{6}$$

And the last step is to optimize the overlapping area and improve the accuracy of interpolation.

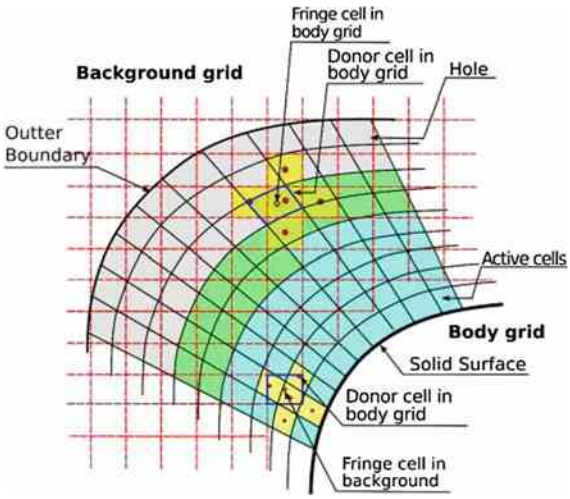

Fig. 2 Diagram of overset grid

dcwan@sjtu.edu.cn

3 The Semi-Submersible Floating Offshore Wind Turbine

3.1 Physical Model

In the present simulation work, a semi-submersible FOWT system, Phase II of OC4 project, is adopted. The FOWT contains several main parts: the NREL 5-MW baseline wind turbine [16], a tower connecting wind turbine and platform, the semi-submersible platform [17], and the mooring system. Figure 3 shows the sketch of this FOWT system, and Table 1 lists the basic properties.

The wind turbine in Phase II of OC4 FOWT system is NERL 5-MW baseline line wind turbine, which is a conventional three-bladed, upwind, variable speed wind turbine. The floating support platform is a semi-submersible floating system which consists of a main column attached to the tower, three offset columns covering significant portion of buoyancy, a couple of smaller diameter pontoons and cross braces to link the main column and offset columns and to strengthen the structure. The semi-submersible floating system for Phase II of OC4 is moored with three catenary lines spread symmetrically about the platform Z-axis (Table 2).

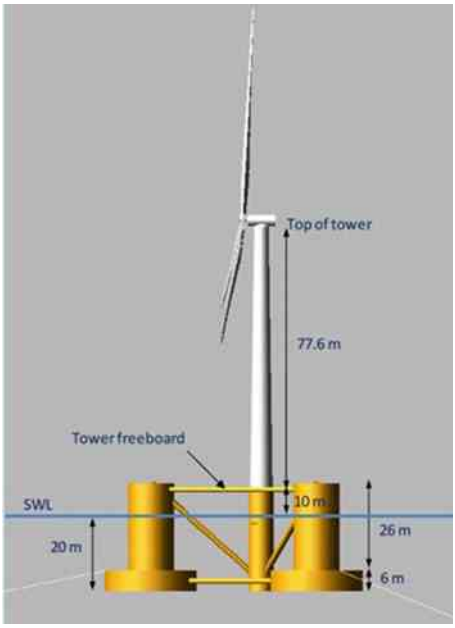

Fig. 3 Phase II of OC4 floating offshore wind turbine system

dcwan@sjtu.edu.cn

Table 1 Specification of the phase II of OC4 FOWT system

Rotor orientation, configuration	Upwind, 3 blades
Rotor, hub diameter	126, 3 m
Hub height	90 m
Rotor mass	110,000 kg
Nacelle mass	240,000 kg
Tower mass	347,460 kg
Coordinate location of CM (rotor, nacelle, and tower)	(−0.2, 0.0, 64.0 m)
Total draft of platform	20 m
Platform mass	1.347E7 kg
Coordinate location of CM (platform)	(0.0, 0.0, −13.46 m)
Number of mooring lines	3
Angle between adjacent lines	120°
Depth to anchors/fairleads below SWL	200 m, 14 m
Radius to anchors/fairleads from platform centerline	837.6, 40.868 m
Unstretched mooring line length	835.5 m
Mooring line diameter	0.0766 m
Equivalent extensional stiffness	7.536 E+8 N
Equivalent mass density/in water	113.35, 108.63 kg/m

Table 2 Structural properties of the FOWT system

Structural mass	1.407E7 kg
CM location below SWL	9.9376 m
Total structure roll inertia about CM	1.1E10 kg m^2
Total structure pitch inertia about CM	1.1E10 kg m^2
Total structure yaw inertia about CM	1.226E10 kg m^2

3.2 Setup of Simulation Domain and Grid Structure

The optimum domain should be large enough to avoid boundary effects. Since the numerical simulations are conducted under the regular wave with wavelength of 156.13 m, the domain is set as cuboid with X (−200 to 400 m), Y (−150 to 150 m), Z (−100 to 240 m), as shown in Fig. 4. As the overset grid technique is utilized, three grid systems are generated, respectively. The green color in Fig. 4 represents for the background mesh covering the whole simulation domain, which is refined along the wave surface to reach grid density requirement for surface capture and also refined near the other two mesh system for better interpolation. The yellow cylinder sub-domain contains the wind turbine including turbine blades, nacelle, and hub. In

dcwan@sjtu.edu.cn

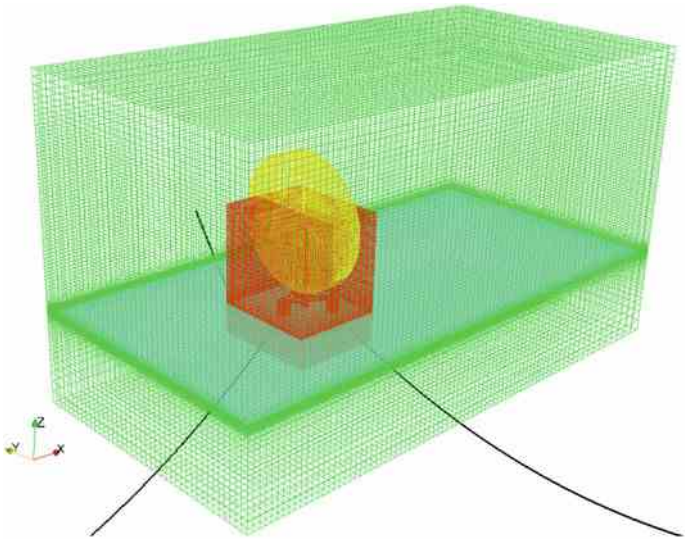

Fig. 4 Simulation domain

this paper, all the solid structures are treated as rigid body, so the red part of grid is generated with the platform and tower.

4 Results and Discussions

In the present work, the fully coupled aero-hydrodynamics of a FOWT in coupling wave-wind conditions are investigated. Two simulations are conducted with same wave condition in which the wave height is 4 m and the wavelength is 156.13 m, while the inlet wind velocities are set as 8 and 11 m/s, respectively. At the beginning of simulation, the platform is fixed until $t = 20$ s, while the wind turbine accelerates from rotating speed 0 rpm to the required speed gradually in 5 s. Comparisons are done on both hydrodynamics and aerodynamics to study the coupling effects between the aerodynamic forces and the hydrodynamic motions.

4.1 Hydrodynamic Responses

In regular heading waves, a moored platform with symmetrically distributed mooring lines oscillates with wave period in three main degrees of freedom (DOFs): surge, heave, and pitch, while the motions in other DOFs are negligible. Despite the hydrodynamic forces on platform, a floating offshore wind turbine is also subject to

dcwan@sjtu.edu.cn

aerodynamic loads mainly on turbine blades. As the turbine rotor is mounted on the top of tower and the tower is fixed on the floating platform, the aerodynamic loads also play essential roles in hydrodynamic responses.

Besides the periodic oscillations corresponding to the wave effect, additional surge motions are also observed in Fig. 5a. With the constraints of mooring system, the effect of aerodynamic loads acts as an additional increase of the equilibrium position. The equilibrium position is determined depending on the aerodynamic loads and the natural properties of the mooring system, where the total forces from the three mooring lines balances out the external loads from the aerodynamics of wind turbine. In Fig. 5a, the red curve shows the surge motion of the FOWT with incoming wind speed set as 8 m/s, and the green one represents for surge motion with wind velocity of $U = 11$ m/s. With rotating speed of rotor increasing with wind speed, the aerodynamic thrust improves significantly just as Fig. 6 shows, thus larger mooring forces are required for the balance. However, the aerodynamic forces are too small compared to the instantaneous wave loads to have obvious influence on the periodic oscillation. Despite the variation on equilibrium position, the oscillating amplitude with wave period does not show much difference with increased inlet wind speed.

The rotating turbine rotor acts as an appendage part of the whole floating offshore wind turbine with both gravity center and rotating center located on the semi-submersible floating platform. So the additional pitching moment from aerodynamics of turbine blades is computed by integral of the moments on each blade surface cell to the rotating center. As the time history of pitch motion shown in Fig. 5c, this additional pitching moment plays a similar role in the pitching motion just as the additional thrust force does in surging motion DOF. Similar conclusions are drawn for the pitching motion.

But it's totally different for heaving component. The main loading effect on this DOF is the additional gravity from the tower and wind turbine, which never changes with working conditions. So the heave curves almost overlap each other despite tiny phase difference.

4.2 Aerodynamic Loads

With different incoming wind velocity from 8 to 11 m/s, the rotational speed of turbine rotor varies from 9.7 to 12.1 rpm, and the averaged aerodynamic thrust increases rapidly from 420 to 710 kN. The time history of aerodynamic thrust is plotted in Fig. 6. Both aerodynamic thrust curves show oscillating regularity with different wave period. Magnification during 260–300 s in right figure tells that the oscillating amplitude with wave period increases with incoming wind speed. This oscillation is resulted from the periodic motions of platform as mentioned above. When turbine blades move toward $+x$ direction with positive velocity component U_x, the relative flow velocity near blades decrease blow the incoming wind speed. On the other hand, when the blades move backward with negative velocity component U_x, the relative

dcwan@sjtu.edu.cn

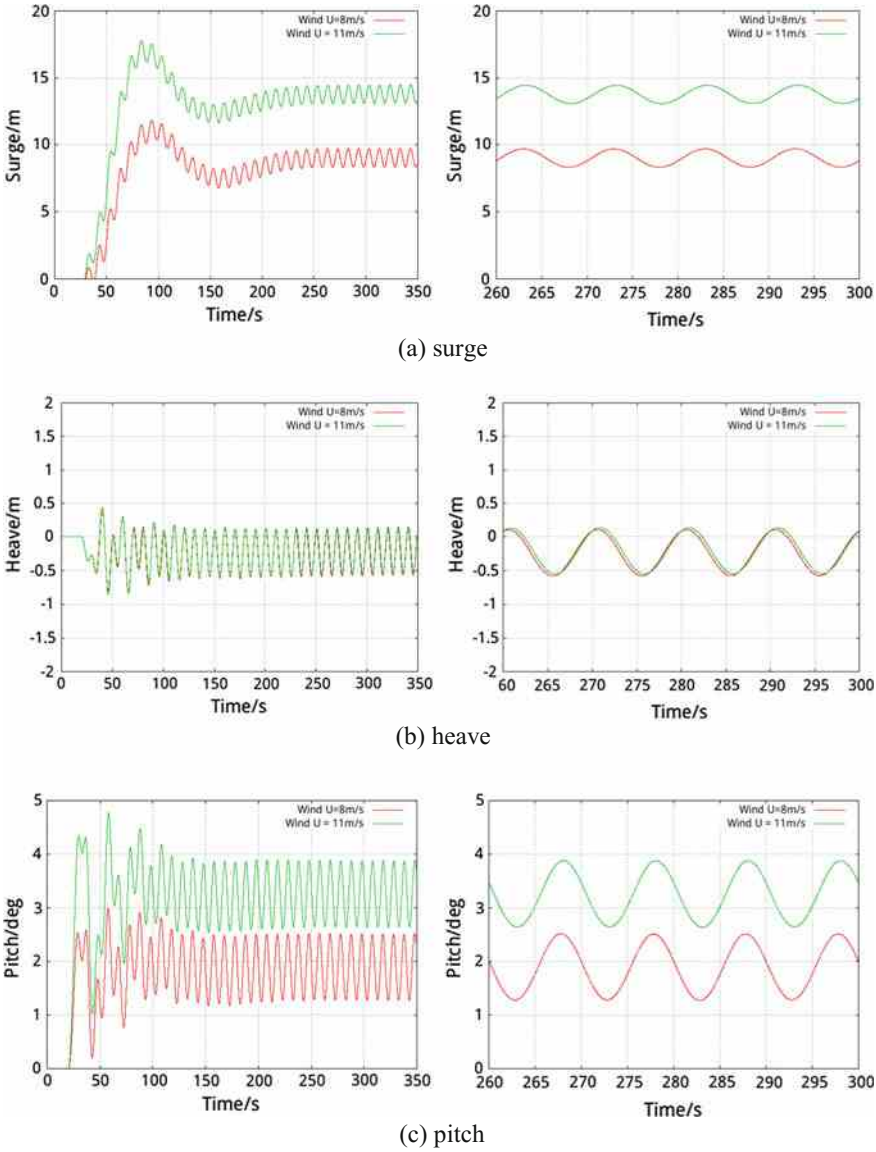

Fig. 5 Hydrodynamic responses of FOWT

flow velocity near blades increases over the inlet wind speed. From curves in the right figure, periodic variation with higher frequency is presented, which results from the tower effect and has a three times frequency of the rotating turbine.

As discussed above, the oscillating amplitudes with wave period differ little with increased inlet wind speed in both surge and pitch DOFs, but significant difference

dcwan@sjtu.edu.cn

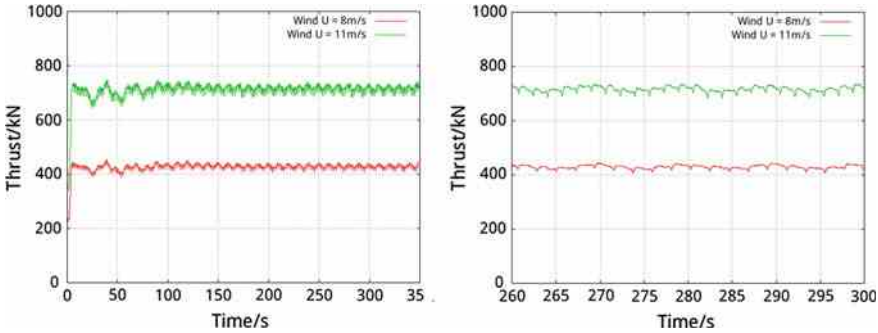

Fig. 6 Aerodynamic thrust on turbine blades

between the oscillating amplitude in two cases are observed in Fig. 6. With careful comparison and analysis, we believe that the key factor should be the pitching angle. To confirm this point of view, more analysis work needs to be done.

4.3 Wake Flow

The spiral wake vortex of turbine blades is generated with two key factors: firstly, incoming flow generates vortex while passing the blade surface. Secondly, the rotating blades disturb the initial uniform wind flow and induce rotating velocity component of the flow around turbine blades. Figures 7 and 8 show the visualization of wake vortex of turbine blades and pressure distribution on platform surface in two cases. The visualized wake vortex is colored by magnitude of velocity. The rotating velocity induced with the rotating blades is quite high near the blades surface, where thin but strong vortex tubes are generated. Interaction with neighbor flow field smooth the flow velocity distribution and leads to the expansion of vortex tube, while the U_x components make the wake vortex shedding downstream, and the finally the spiral vortex is generated. Because of the additional motion of turbine blades in sync with platform, the induced flow velocity also varies periodically. So the distance between two neighbor vortex cubes is not exactly the same.

The platform surface is colored with pressure distribution. Four figures in Fig. 7 or Fig. 8 represents for four moments during one wave period: the platform reached the minimum pitch position at $t = 263$ s, then moves to the equilibrium position at $t = 265.5$ s, then keeps moving until $t = 268$ s to the maximum pitching position, then turns back again and moves to the equilibrium position at $t = 270.5$ s, in the next quarter of cycle, the FOWT arrives at the minimum pitch position again, then round and round. The pressure distribution shows the immersed height of cylinders and the periodic pitching and heaving motions, also indicates the variations of hydrodynamic loads. Because of the pitching effect, the immersed area of downstream cylinder is

dcwan@sjtu.edu.cn

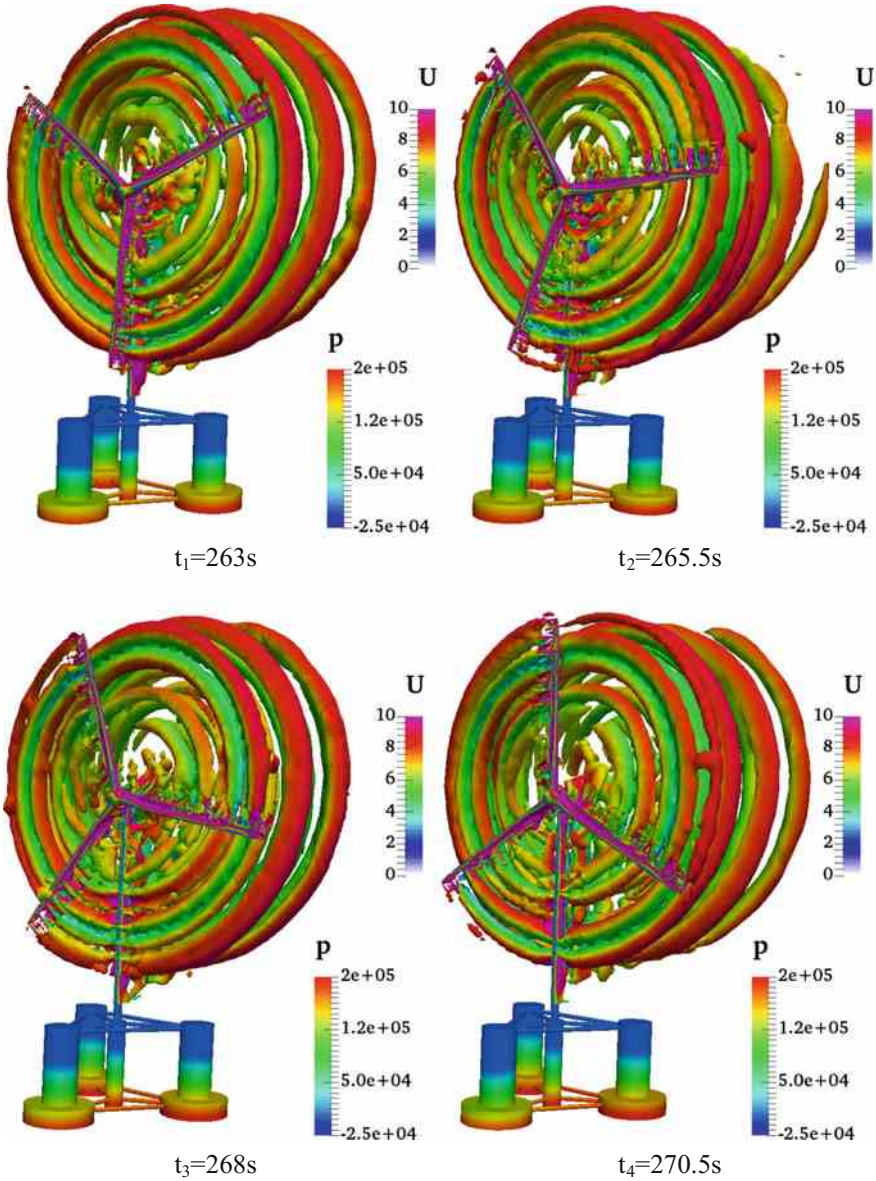

Fig. 7 Visualization of wake vortex of turbine blades and pressure distribution on surface of platform with inlet wind speed $U = 8$ m/s

much larger than that of the upstream one, and more significant difference is observed with higher inlet wind speed.

dcwan@sjtu.edu.cn

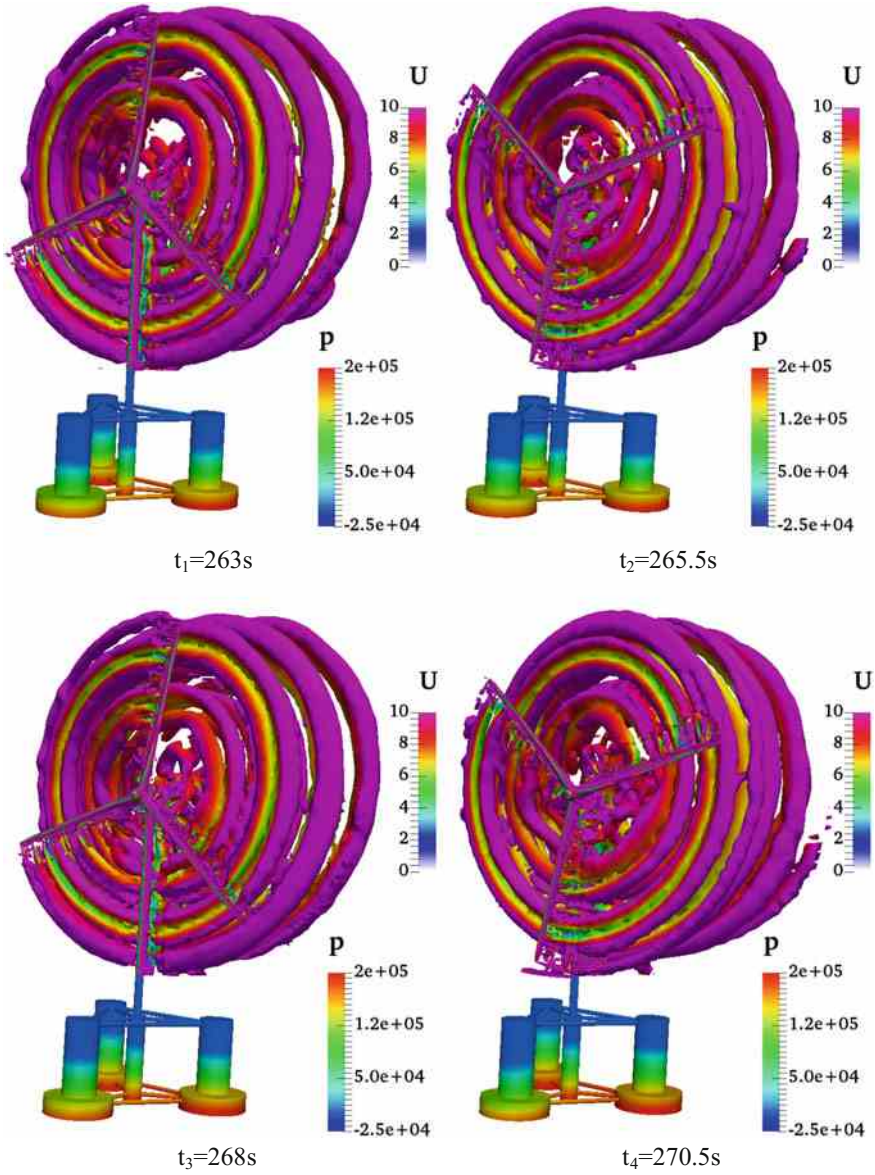

Fig. 8 Visualization of wake vortex of turbine blades and pressure distribution on surface of platform with inlet wind speed $U = 11$ m/s

dcwan@sjtu.edu.cn

5 Conclusions

The fully coupled aero-hydrodynamic simulation of the Phase II of OC4 FOWT system is conducted. The in-house code naoe-FOAM-SJTU solver, based on OpenFOAM and coupled with overset grid technology, is employed. The additional aerodynamic forces on turbine blades mainly effect the equilibrium position of the FOWT system in surge and pitch DOFs. When the aerodynamic forces on turbine blades increase with rotating speed as well as the inflow wind velocity, the new equilibrium position gets further from the initial one, in which case larger mooring forces are required for force balancing. But the oscillating amplitude with wave period does not show much difference with increased inlet wind speed, because the aerodynamic forces are too small compared to the instantaneous wave loads to have obvious influence on the periodic oscillation.

The periodic motion of blades in sync with platform causes the variations of the relative flow velocity near blades surface. So the aerodynamic thrust on turbine blades shows periodic oscillating regularity with wave period same as the platform motion period. Besides, the oscillating amplitudes increase with inlet wind speed is observed, and we believe that the key factor should be the equilibrium pitching angle. To confirm this point of view, more analysis work needs to be done.

Detailed flow information also clarities the flow fields and indicates the coupling effects. Due to the axial exponent of flow velocity inherited from the inlet flow and the rotational component induced with rotating blades, series of spiral wake vortex are generated and shedding downstream. For the semi-submersible floating platform, because of the equilibrium pitching angle resulted from the additional aerodynamic forces, the immersed area of downstream cylinder is much larger than that of the upstream one.

Acknowledgements This work is supported by the National Natural Science Foundation of China (51879159, 51490675, 11432009, 51579145), Chang Jiang Scholars Program (T2014099), Shanghai Excellent Academic Leaders Program (17XD1402300), Program for Professor of Special Appointment (Eastern Scholar) at Shanghai Institutions of Higher Learning (2013022), Innovative Special Project of Numerical Tank of Ministry of Industry and Information Technology of China (2016-23/09) and Lloyd's Register Foundation for doctoral student, to which the authors are most grateful.

dcwan@sjtu.edu.cn

References

1. Wang CM, Utsunomiya T, Wee SC, Choo YS (2010) Research on floating wind turbines: a literature survey. IES J Part A: Civil Struct Eng 3(4):267–277
2. Skaare B, Nielsen FG, Hanson TD (2015) Analysis of measurements and simulations from the Hywind Demo floating wind turbine. Wind Energy 18(6):1105–1122
3. BBC (2015) Floating wind farm to be installed off Peterhead. Available from: http://www.bbc.co.uk/news/uk-scotland-scotland-business-34694463
4. Viselli AM, Goupee AJ, Dagher HJ (2015) Model test of a 1:8-scale floating wind turbine offshore in the gulf of maine. J Offshore Mech Arct Eng 137(4):041901
5. Koo BJ, Goupee AJ, Kimball RW (2014) Model tests for a floating wind turbine on three different floaters. J Offshore Mech Arct Eng 136(2):020907
6. Cordle A (2010) State-of-the-art in design tools for floating offshore wind turbines. Deliverable report Under (SES6), UpWind project, Bristol, UK, Contract
7. Sebastian T, Lackner MA (2013) Characterization of the unsteady aerodynamics of offshore floating wind turbines. Wind Energy 16(3):339–352
8. Jonkman JM (2009) Dynamics of offshore floating wind turbines—model development and verification. Wind Energy 12(5):459–492
9. Liu Y, Xiao Q, Incecik A, Incecik A, Peyrard C, Wan DC (2017) Establishing a fully coupled CFD analysis tool for floating offshore wind turbines. Renew Energy 112:280–301
10. Tran TT, Dong HK (2015) The aerodynamic interference effects of a floating offshore wind turbine experiencing platform pitching and yawing motions. Indian J Thorac Cardiovasc Surg 29(2):549–561
11. Li PF, Cheng P, Wan DC (2015) Numerical simulations of wake flows of floating offshore wind turbines by unsteady actuator line model. In: Proceedings of the 9th international workshop on ship and marine hydrodynamics, Glasgow, UK, 26–28 August
12. Menter FR (1994) Two-equation eddy-viscosity turbulence models for engineering applications. AIAA J 32(8):1598–1605
13. Shen Z, Wan D (2016) An irregular wave generating approach based on naoe-FOAM-SJTU solver. China Ocean Eng 30(2):177–192
14. Cao H, Wan D (2014) Development of multidirectional nonlinear numerical wave tank by naoe-FOAM-SJTU solver. Int J Ocean Syst Eng 4(1):52–59
15. Carrica PM, Huang J, Noack R (2010) Large-scale DES computations of the forward speed diffraction and pitch and heave problems for a surface combatant. Comput Fluids 39(7):1095–1111
16. Jonkman J, Butterfield S, Musial W, Scott G (2009) Definition of a 5-MW reference wind turbine for offshore system development. National Renewable Energy Laboratory, Golden, CO
17. Robertson A, Jonkman J, Masciola M (2012) Definition of the semisubmersible floating system for phase II of OC4. Offshore Code Comparison Collaboration Continuation (OC4) for IEA Task, 30

dcwan@sjtu.edu.cn